FULL PAPER

ADVANCED FUNCTIONAL MATERIALS

Assembly of Photopolymerizable Discotic Molecules on an Aligned Polyimide Layer Surface to Form a Negative Retardation Film with an Oblique Optical Axis**

By *Jason J. Ge*, *Seok-Choel Hong*, *Benjamin Y. Tang*, *Christopher Y. Li*, *Dong Zhang*, *Feng Bai*, *Bart Mansdorf*, *Frank W. Harris*, *Denke Yang*, *Yuen-Ron Shen*,* and *Stephen Z. D. Cheng**

Ultraviolet (UV) polymerizable discotic liquid-crystalline (DLC) molecules (2,3,6,7,10,11-hexakis(4′-acryloy-*m*-alkyloxybenzoyoxy)triphenylene [HAHBT-*m*, where *m* was the number of methylene units, and here $m = 6$ (HAHBT-6)]) were assembled to form a negative retardation film with an oblique optical axis on a specifically designed rubbing-aligned polyimide layer surface [6FDA-11CBBP (where 11 is the number of methylene units in the side chains)]. The side chains of this polyimide were terminated by cyanobiphenyl groups. Surface-enhanced Raman scattering (SERS) and optical second harmonic generation results showed that rubbing caused a surface structural re-arrangement in the alignment layer resulting in a negative pre-tilt angle (θ_s) of –8.5° (which was in the direction opposite to the rubbing direction). The molecular topology at the rubbed surface was governed by a stable fold-like bent structure of the cyanobiphenyl side chains, in which the CN groups preferentially pointed down towards the surface. When the DLC molecules were deposited onto the alignment surface and polymerized via UV irradiation to generate a new optical film, an oblique optical axis with an average tilt angle of –18.6° with respect to the film normal was detected using ellipsometric measurements. This tilted optical axis was developed by the DLC molecules being wedged on top of the cyanobiphenyl groups when in the bent conformation. Furthermore, the tilt angle difference between the θ_s at the alignment surface and at the air interface of the DLC molecules was attributed to a splay deformation of the DLC molecules along the film surface normal. Optical modeling has also confirmed our experimental observations.

1. Introduction

A variety of high-resolution thin film transistor liquid-crystal displays (TFT-LCDs) have been developed and commercialized in laptop computers, desktop monitors, and other mobile telecommunication devices.[1,2] However, the problems of narrow viewing angles, gray-scale inversion, and color distortion in the addressed state (the electric field-on state) have prevented their use in large LCD television screens. The compensation of the angular dependence of the birefringence in the addressed state of conventional TFT-LCDs requires an optimized optical retardation film that possesses both a negative birefringence and an oblique optical axis. In addition, to maintain a high contrast ratio, this retardation film must not degrade the transmission of the polarized light from the addressed state. The early polymer optical retardation films with improved viewing angles were prepared using reactive rod-like LCs obtained through in-situ photopolymerization in both nematic and smectic phases.[3,4] Other technologies to improve viewing angles were also developed that include in-plane switching (IPS) modes, multi-domain vertically aligned (MVA) modes, and optically compensated bent (OCB) modes.[5–7] The IPS mode can possess wide viewing angle optical performance with a uniaxial positive optical retardation film. In the MVA and OCB modes, high-quality negative optical retardation films are necessary for improving the optical performance of the addressed-state and suppressing light leakage.

Since the discovery of columnar phases in discotic liquid crystals (DLCs) in 1977,[8] significant attention has been paid to this class of new materials resulting in applications such as nanowires for one-dimensional (1D) transport processes in photoconduction,[9–11] photovoltaics,[12,13] and light-emitting diodes (photoluminescence).[14] In general, DLC molecules possess a planar rigid core coupled with flexible aliphatic tails. The cores usually consist of a single phenylene, triphenylene, metallic complex, or hydrogen-bonded disc structure.[8,15–23] Therefore, when the DLC molecules "lie down" on a substrate,[22,23] the molecules intrinsically exhibit uniaxial negative birefringence due to the fast photon transport along the direction normal to the disc (the optical axis $\vec{n}$). Furthermore, the

[*] Prof. S. Z. D. Cheng, Dr. J. J. Ge, Dr. B. Y. Tang, Dr. D. Zhang, Dr. F. Bai, Dr. B. Mansdorf, Dr. F. W. Harris
Maurice Morton Institute and Department of Polymer Science
The University of Akron
Akron, OH 44325-3909 (USA)
E-mail: scheng@uakron.edu
Prof. Y.-R. Shen, Dr. S.-C. Hong
Department of Physics, University of California Berkeley
Berkeley, CA 94720-7300 (USA)
E-mail: shenyr@socrates.berkeley.edu
Prof. C. Y. Li
Department of Materials Science Engineering, Drexel University
Philadelphia, PA 19104 (USA)
Prof. D. Yang
Liquid Crystal Institute, Kent State University
Kent, OH 44 010-0001 (USA)

[**] This work was supported by the NSF DMR-0203 994, the Collaborative Center in Polymer Photonics between AFRL Materials and Manufacturing Directorate and The University of Akron, and Nitto Denko (USA).

  DOI: 10.1002/adfm.200304365 *Adv. Funct. Mater.* **2003**, *13*, No. 9, September

ADVANCED FUNCTIONAL MATERIALS

optical retardation is tunable by varying the DLC film thickness and/or the anisotropic refractive indices.[24,25]

Recently, an approach was proposed to generate a uniaxial negative retardation film with an oblique optical axis. This approach utilized an arrangement of ultraviolet (UV) polymerizable DLC molecules on a commercially available alignment layer surface or a SiO_2 vapor deposition surface with an oblique alignment.[26–29] UV exposure then induces crosslinking reactions in the DLCs to generate negative birefringence retardation films with an oblique optical axis. However, the oriented molecular structure and formation mechanisms of the DLC on the aligned surfaces are not currently clear.

In this investigation we have specifically designed a system to study the formation mechanisms of the negative birefringence retardation films with an oblique optical axis. Optical second harmonic generation (SHG) and surface enhanced Raman scattering (SERS) techniques were used, both of which are intrinsically sensitive in characterizing molecularly anisotropic surfaces.[30–35] The technique of SHG is capable of probing the orientation of polar groups at the surface,[30–34] while SERS is capable of detecting surface chemical structural orientations adjacent to silver colloidal layers.[33,35] The linear optical property changes were examined using an ellipsometer to determine the precise tilt angles of the optical axes in the films. Optical modeling was also used to calculate the anisotropic behavior of the films.

There were two steps in this investigation. In the first step, a newly designed aromatic polyimide containing cyanobiphenyl groups in the side chains was synthesized to generate alignment layers with high average negative tilt angles (θ_b) in LCDs. The θ_b is defined as the angle between the long molecular axis of the LC molecules and the film surface plane. The θ_b was opposite of the rubbing direction in this polyimide, which is different from other commercially available alignment layer materials (see Fig. 1).[33,34] It has been deduced that the negative θ_b was caused by the negative surface pre-tilting angles (θ_s) generated at the surface of the alignment layer. In this paper, we will focus on how the cyanobiphenyl side chains arrange at the surface after rubbing and what molecular mechanism is involved in the formation of the θ_s.

In the second step, we assembled photopolymerizable triphenylene-based DLC molecules on the newly developed alignment layer surface with the expectation that these DLC molecules would also be aligned by the θ_s. After UV-polymerization, a polymer film was formed on top of the alignment layer. The chemical structure of DLC and its transmission spectrum in the visible light region can be seen in Figure 2 (see also Experimental section). Detailed fabrication procedure of the alignment layer and the negative compensation film with an oblique optical axis is shown in Figure 3 (see also Experimental section). The question we will try to answer is how the DLC molecules orient on the rubbed surface in forming a negative retardation film with an average oblique optical axis (ϕ_{om}), which is defined as the angle between the optical axis and the

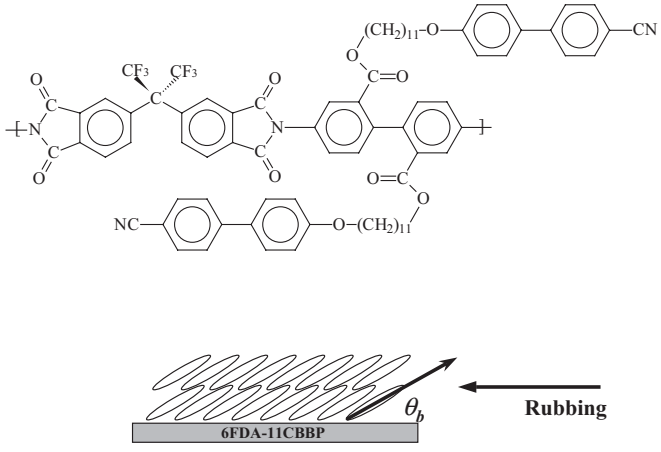

Fig. 1. LC bulk tilt angles ($-\theta_b$) induced by rubbing on the alignment thin film of 6FDA-11CBBP, along with its chemical structure. Schematic drawing of LCs oriented on the alignment surface having a negative tilt angle orientation with respect to the rubbing direction.

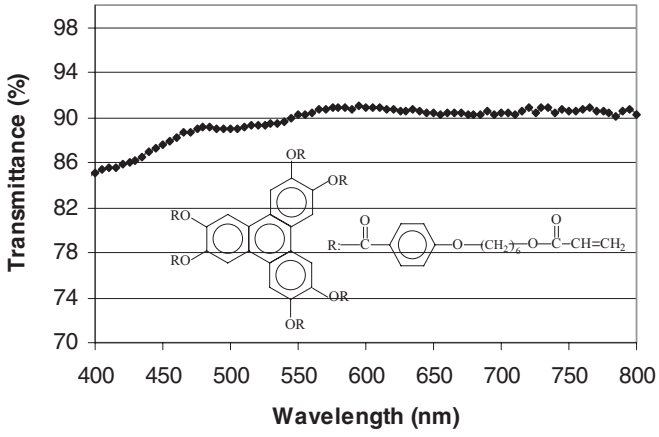

Fig. 2. Transmission spectrum of photocrosslinked DLC HABAT-6 in the visible region, along with the inset of the chemical structure of the crosslinkable DLC HABAT-6 molecules.

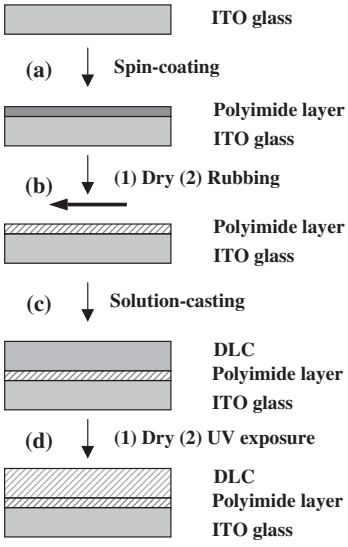

Fig. 3. Schematic of the fabrication processes of the DLC-based oblique negative optical film on the rubbed polyimide alignment surface: a) Spin-coating of the polyimide alignment layer onto ITO glass substrates. b) Mechanical rubbing of the alignment surface after the alignment layer was dried. c) Solution-casting of the DLC molecules onto the alignment surface. d) UV exposure after the DLC coating was dried.

film surface normal. The absolute value of this angle ϕ_{om} is equal to the average tilt angle of the DLC molecules (θ_{om}) or the angle between the DLC plane and the film surface. The correlation between the θ_s at the alignment layer surface and the tilt angle at the air interface (θ_{air}) in the bulk DLC molecules is also discussed. Finally, we performed optical modeling to confirm our experimental observations.

2. Results and Discussion

2.1. 6FDA-11CBBP Alignment Behavior and Surface Molecular Orientation

Based on magnetic null measurements of the LC cells having an anti-parallel configuration with respect to the rubbing direction, the 6FDA-11CBBP (synthesized from 2,2′-bis(3,4-dicarboxyphenyl)hexafluoropropane dianhydride (6FDA) and 2,2′-bis{ω-[4-(4-cyanophenyl)phenyoxy]-11-alkoxycarbonyl]}-4,4′-biphenyl diamine (11CBBP, where 11 is the number of methylene units in the side chains), and abbreviated as 6FDA-11CBBP; see Fig. 1 for structure) alignment layer exhibited a unique characteristic feature in generating a high negative θ_b of $-45 \pm 5°$ for bulk 5CB LC molecules. Note that alignment layers made of the same aromatic polyimide (6FDA-PFMB) backbone but missing the cyanobiphenyl side chains only provide a θ_b of 1–2°. This implies that the cyanobiphenyl side chains in 6FDA-11CBBP play a critical role in generating the high θ_b alignment on the LC bulks. Furthermore, the 6FDA-11CBBP studied here possesses a higher θ_b than 6FDA-6CBBP (the same polymer but only having six methylene units in the side chains instead of eleven).[33] In addition, an ester linkage in 6FDA-*n*CBBP also leads to a higher θ_b compared to that in 6FDA-*n*CBO with an ether linkage.[34,35] Therefore, it has been concluded that both the number of methylene units in the side chains and the type of chemical linkage between the side chains and the backbones affect θ_b.

A Raman spectrum of the bulk 6FDA-11CBBP (40 μm thick) is shown in Figure 4a, which serves as a reference to identify the characteristic vibrational bands observed in the corresponding SERS spectra. Based on the standard band assignments,[36] the characteristic bands of the polyimide backbones at 1782 cm^{-1} and 1380 cm^{-1} are associated with the C=O stretching and the axial C–N–C stretching, respectively. The aromatic ring stretching in the backbones at 1621 cm^{-1} overlaps the intense biphenyl ring stretching at 1606 cm^{-1} of the cyanobiphenyls in the side chains. Aromatic C–H stretching at 3065 cm^{-1} and the C_6H_4 ring stretching at 1523 cm^{-1} were also observed. Another cyanobiphenyl vibrational band was identified at 2227 cm^{-1} as the CH_4–CN stretching, a C–C bridge stretching at 1290 cm^{-1}, and C–H in-plane bending (in CH_4) at 1182 cm^{-1}. The characteristic $\nu(CH_2)$ bands were 2895 cm^{-1}, 2861 cm^{-1} (asymmetric and symmetric CH_2 stretching, respectively), and 1442 cm^{-1} (CH_2 deformation).

The SERS spectrum of an unrubbed polyimide thin layer surface (Fig. 4b) exhibited considerably weaker signals than the rubbed polyimides (Fig. 4c) except for the methylene units. In particular, the bands at 2228 cm^{-1}, 1606 cm^{-1}, 1291 cm^{-1}, 1183 cm^{-1}, and 1786 cm^{-1} were much weaker in the unrubbed films. Based upon the SERS selection rules,[37] without rubbing, only methylene units in the side chains are rich at the surface, and both the polyimide backbones and the cyanobiphenyls in the side chains possess an almost in-plane orientation.

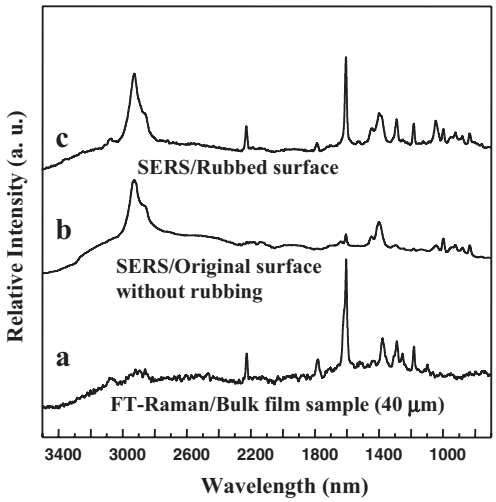

Fig. 4. A Raman scattering spectrum of the bulk film (40 μm-thickness) (a), two SERS spectra of 6FDA-11CBBP without mechanical rubbing (b) (with silver colloidal deposition), and with mechanical rubbing (c) (with silver colloidal deposition).

Figure 4c shows a SERS obtained from a rubbed 6FDA-11CBBP thin-layer surface. The signals from the CH_4–CN stretching (2228 cm^{-1}), the biphenyl ring stretching (1606 cm^{-1}), the C–C bridge stretching (1291 cm^{-1}), and the C–H in-plane bending (1183 cm^{-1}) of the cyanobiphenyls in the side chains were dramatically enhanced. Again, based upon the SERS selection rules,[37] the existence of a tilted orientation of the cyanobiphenyl side chains at the rubbed surface was suggested. In addition, the imide C=O stretching (1786 cm^{-1}) in the backbones was also detected after rubbing, indicating that the imide–phenyl conjugated structure adopted a tilted conformation at the aligned layer surface. These results qualitatively show that both the side chains and the backbones at the surface reorient during the rubbing process. It is conceivable that the cyanobiphenyl side chains in this polyimide govern the surface structural orientation and topology.

2.2. Anisotropic Orientation of the Cyanobiphenyl Groups at the Rubbed Surface

When the cyanobiphenyls of the polyimide layer are uniaxially oriented by the rubbing procedure, a significant polarization angular dependence of these cyanobiphenyls with the input–output combinations of S/P polarizations can be observed in SHG measurements. This observation can provide quantitative information on the anisotropic tilted orientation of these cyanobiphenyls at the aligned layer surfaces. The SHG data fitting obtained from the rubbed 6FDA-11CBBP surfaces allowed us to determine six independent non-vanishing elements of $\chi^{(2)}_{CBBP}$. The corresponding values are: $\chi^{(2)}_{xxx}/\chi^{(2)}_{xyx}/\chi^{(2)}_{xzz}/\chi^{(2)}_{zxx}/\chi^{(2)}_{zyy}/$

ADVANCED FUNCTIONAL MATERIALS

$\chi^{(2)}_{zzz}$ = 1:0.2:0.032:–0.27:–0.16:–0.089 (errors of ±5 %, ±20 %, ±5 %, ±8 %, and ±10 %). The cyanobiphenyl orientation parameters at the surface were deduced to be $\theta_0 = 81.5°$, $\sigma = 13.0$, $d_1 = -0.69$, $d_2 = 0.49$, and $d_3 = -0.31$. Note that the negative d_1 value suggests an opposite alignment of cyanobiphenyls with respect to the rubbing direction. The surface pretilt angle θ_s of cyanobiphenyls in the side chains was $-(90° - 81.5°) = -8.5°$, and was surprisingly low compared with the average tilting angle θ_b measured using bulk 5CB LC molecules.

The question that arises from the SHG observations is: how do the tilted cyanobiphenyls orient at the surface? Two possible tilt arrangements of the cyanobiphenyl orientation on the surface are proposed: one with the CN groups pointing down towards the rubbed surface, and another with the CN groups pointing away from the surface. The SHG experiments previously described cannot distinguish between these two possible orientations, and a SHG phase measurement was needed. This experiment utilizes a comparison of the SHG phase of $\chi^{(2)}_{xxx}$ of 6FDA-11CBBP with that of 5CB monolayer adsorbed on a commercial P6 polyimide alignment surface that does not contain side chains. As shown in the interference patterns of these two cases in Figure 5, the measured SHG phases of $\chi^{(2)}_{xxx}$ from 6FDA-11CBBP (Fig. 5a) and 5CB monolayer adsorbed on the P6 surface (Fig. 5b) exhibited opposite phase behaviors in $\chi^{(2)}_{xxx}$. Therefore, the cyanobiphenyls at the surface can be assumed to adopt a tilted arrangement where the CN groups point down towards the rubbed surface, as illustrated in Figure 5c. This conclusion was based on the reference that the 5CB monolayer absorbed on the P6 surface was oriented with the CN groups pointing down towards the surface, as seen in Figure 5d.[33] If the cyanobiphenyls in the side chains of 6FDA-11CBBP pointed upwards, the measured SHG phase of $\chi^{(2)}_{xxx}$ from 6FDA-11CBBP would have to be identical to that of 5CB monolayer adsorbed surface. Therefore, combined with the methylene units in the side chains, a fold-like bent structure of the side chains must form at the rubbed surface. Furthermore, since only the cyanobiphenyls in this structure can provide physical interactions with the LC molecules (such as 5CB used here), the negative θ_s formed at the surface was responsible for the generation of the θ_b in the LC bulks. In the past, a molecular interaction between calamitic LC groups and DLC molecules was reported. It was shown that photo-aligned cyanoazobenzene groups included in a polymer layer were capable of determining the anisotropic orientation of DLC molecules containing a triphenylene skeleton.[38]

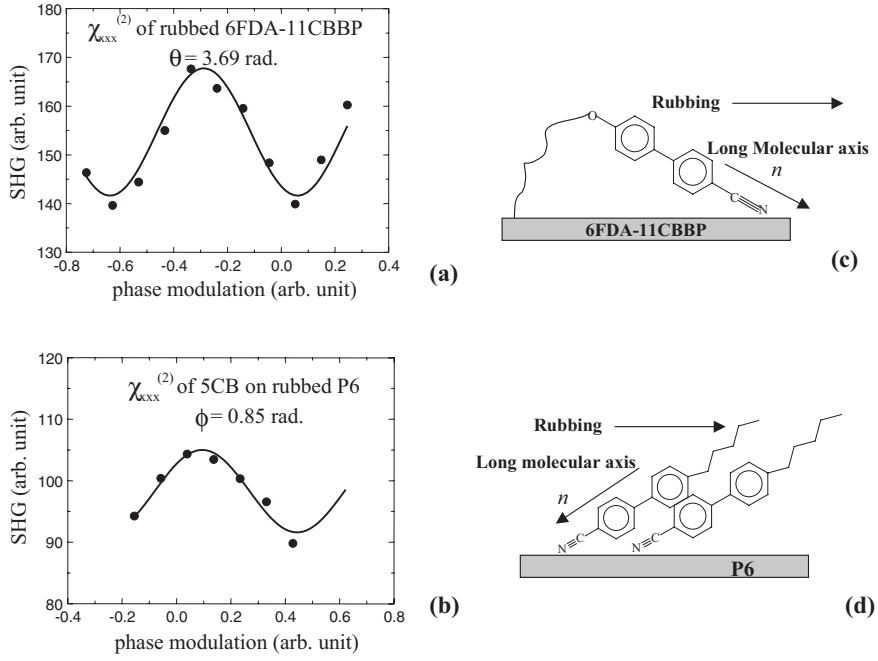

Fig. 5. Experimental data points and the fitting curves in a,b) represent the SHG phase measurements of $\chi^{(2)}_{xxx}$ on the 6FDA-11CBBP thin film surface after rubbing and 5CB monolayer absorbed on the rubbed P6 alignment surface. Schematic models of the molecular orientation of c) a fold-like tilt conformation of the cyanobiphenyls on the rubbed surface of 6FDA-11CBBP, and rubbing direction is represented by an arrow; and d) a 5CB LC monolayer absorbed on the P6 alignment surface, in which the CN groups point down towards the layer surface and the θ_s (positive) is along the rubbing direction.

2.3. Assembly of DLC Molecules on the Alignment Surface and Their Optical Behavior

After the DLC molecules were exposed to UV light, a polymer film was produced on top of the alignment layer that possessed an oblique optical axis. Figure 6 shows the results of the optical anisotropy of this film measured by ellipsometric experiments (the solid circles in this figure). A relationship between the effective retardation, ΔL_{eff}, (see below in Eq. 4) and the incident angle α_0 of the light with respect to the film surface normal (see the insert of Fig. 6) can be established. In

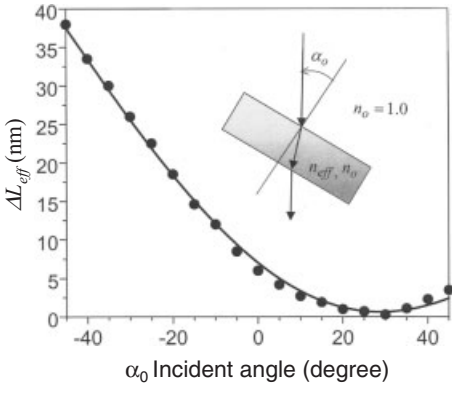

Fig. 6. An effective optical retardation ΔL_{eff} of the oblique retardation optical film made of the crosslinked HABAT-6 DLC molecules as a function of the incident angle (α_0) in ellipsometric measurements. The experimental data are shown as solid dots, and the line was based on the calculation of the optical modeling.

these measurements, the ΔL_{eff} values resulted from the anisotropic negative optical ellipse in the film ($n_0 > n_e$). The minimum retardation occurred at an incident angle of $\alpha_{om} = 30°$, indicating that the angles between the DLC molecular director, $\vec{n}$, and the film surface normal were not a constant. The average angle between the DLC plane and the film surface should be $\alpha_{om} = \sin^{-1}[\sin\alpha_{om}/(n_e + 2n_0)/3] = 18.6°$ (and this angle has a negative sign).

The orientation of the DLCs in this film was investigated using wide-angle X-ray diffraction (WAXD) techniques. Figure 7a shows a 2D WAXD pattern of a freestanding, UV-polymerized DLC film that was (carefully) separated from the alignment/ITO glass substrate. The X-ray incident beam was aligned with an edge-on mode of the film along the film rubbing direction but with a preset 18° rotation angle along the z-axis, as shown in the insert of Figure 7a. Note that the z-axis was parallel to the film surface and perpendicular to the rubbing direction. This WAXD experimental set-up was based on the ellipsometric result of $\theta_{om} = -18.6°$, and we attempted to make the X-ray beam irradiate the sample nearly parallel to the average disc plane of the DLC molecules.

As shown in Figure 7a, a pair of diffuse scattering arcs in the high 2θ angle region were observed on the equator. The d-spacing was ~0.47 nm, (the azimuthal scan profile is shown in Fig. 7b) which represented the average distance between stacked DLC molecules[21] as well as possible peripheral alkyl-chain separation. Therefore, the planes of the discotic cores were oriented parallel to the X-ray beam. In the low 2θ region, there were two pairs of diffraction arcs that were centered at $2\theta = 3.4°$ with almost equal intensities. The corresponding d-spacing was 2.59 nm. These two pairs of diffraction arcs were in the quadrants at angles of ±53° off the equatorial direction as shown in the azimuthal scan in Figure 7c. This suggests the existence of a columnar nematic phase in the DLC film, in which the basic rigid-core unit was formed by the stacking of many DLC molecules. The column direction was tilted away from the disc normal at angles of ±37° (two kinds of column orientations with a tilting angle of 37° or –37°). Since 2.99 nm represented the spacing of the columns perpendicular to the columnar axis, the diameter of the DLC molecules parallel to the discs was calculated as 3.74 nm. A schematic illustration of the DLC molecules arranged in the films is shown in Figure 7d. Edge-on WAXD experiments on the sample with rotations around the z-axis other than 18° only generated asymmetrical diffraction arcs in both the high and low 2θ angle regions.

The assembled DLC molecules arranged on the rubbed surface are schematically illustrated in Figure 8. In this figure, the fold-like bent structure generates a negative θ_s at the polyimide alignment layer surface, and we assume that this angle translates as the tilting angle of the first layer of the DLCs that are in contact with the alignment layer surface (see below for the validity of this assumption). The negative θ_{air} is the tilting angle of the DLCs at the top layer surface in contact with the air, and the negative θ_{om}

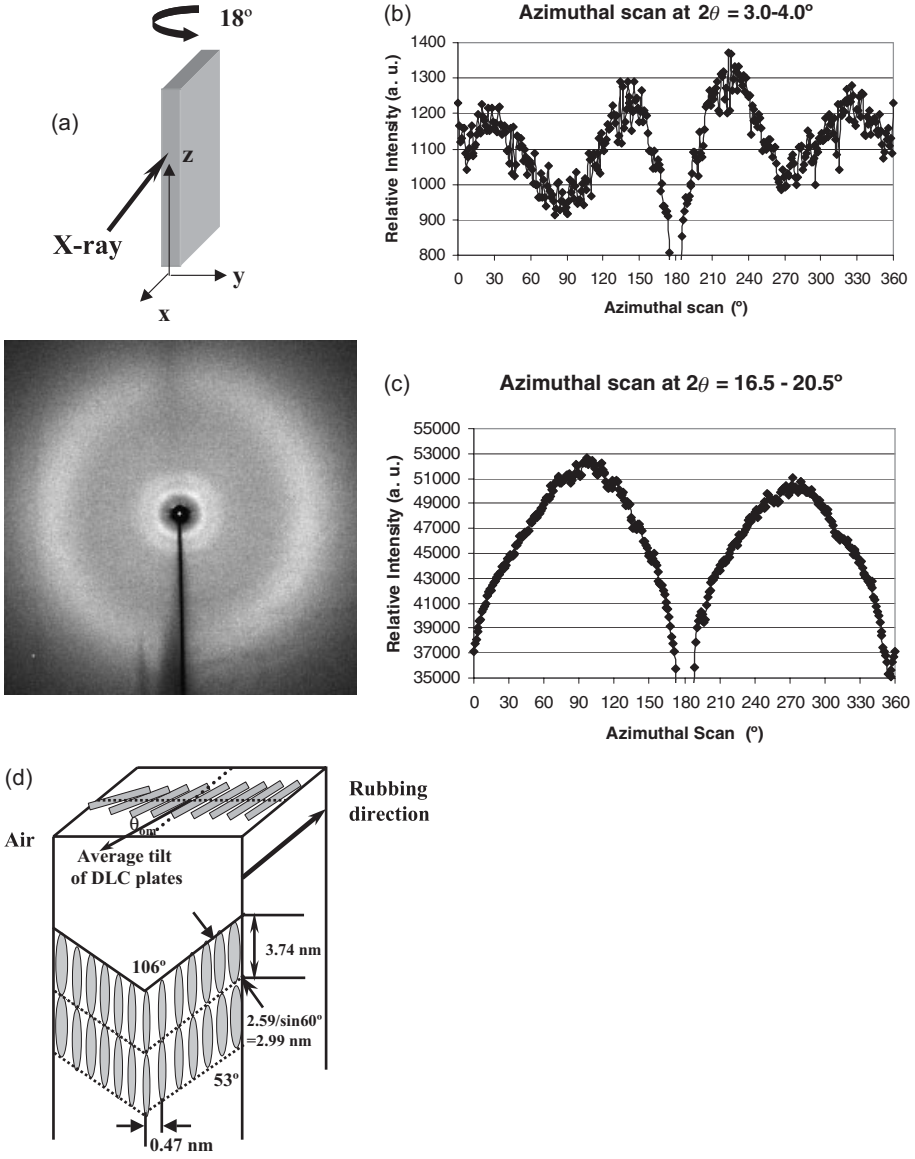

Fig. 7. a) A 2D WAXD pattern of a film, of which the oriented HABAT-6 DLC molecules are induced by the polyimide alignment surface, obtained after the rotation of 18° away from the rubbing direction (along the z-axis). Note that the X-ray beam was parallel to the rubbing direction before the rotation. b) The azimuthal scan of the WAXD pattern shown in Figure 6a at the d-spacing of 0.47 nm. c) The azimuthal scan of the WAXD pattern in Figure 6a at the d-spacing of 2.59 nm. d) A schematic illustration of the DLC molecular orientation in the film in real space.

ADVANCED FUNCTIONAL MATERIALS

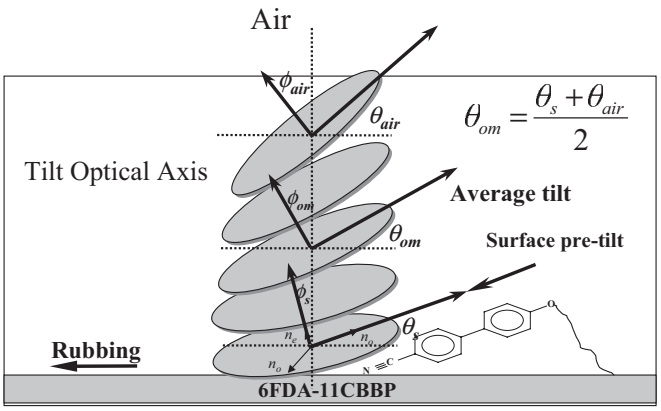

Fig. 8. A schematic representation of the orientation of the HABAT-6 DLC molecules on the alignment surface made of 6FDA-11CBBP showing the surface tilting angle (θ_s) from the fold-like bent structure on the polyimide alignment surface and the mean tilting angle (θ_{om}) of the DLC plates in the optical film as well as the plate tilting angle ($\theta_{air} = 2\theta_m - \theta_s$) at the air/DLC surface, along with the optical axis of ϕ_{om}, ϕ_s, and ϕ_{air}.

is the average angle between the θ_s and θ_{air} [$\theta_{om} = (\theta_s + \theta_{air})/2$] in the film. The optical axis $\vec{n}$ is always perpendicular to the disc plane of the DLCs, and the angle between this axis and film surface normal is defined as ϕ. Therefore, corresponding to those θ_s, θ_{om}, and θ_{air}, we have ϕ_s, ϕ_{om}, and ϕ_{air}, and their values were identical to those θ_s.

It is evident that there is a difference between the θ_s of –8.5°, which was determined directly by the SHG measurements and the θ_{om} of –18.6° calculated from the ellipsometric measurements. Assuming that the difference was attributed to a linear splay of the DLC molecules along the film surface normal direction, the θ_{air} of the DLC molecules in the optical film can be calculated based on the equation of $\theta_{air} = 2\theta_{om} - \theta_s = -29.1°$. Therefore, the optical axis of the DLC molecules (ϕ_{air}) was 29.1° away from the film surface. The formation of the larger θ_{air} was possibly due to the surface anchoring energy changes, which are proportional to the distance from the alignment layer surface to the air surface. This constructs a splay deformation of the DLC molecules along the film surface normal. It is also important to note that the disc plane of the DLC molecules was oriented in a direction opposite to the rubbing direction. This can be explained by the fact that only the cyanobiphenyls in the fold-like bent structure provided physical interactions with the DLC molecules. In this case, the DLC molecules were wedged onto the cyanobiphenyl side chains of the fold-like bent structures at the surface. Therefore, the formation mechanism of this DLC molecular orientation must be associated with an interaction between the DLC molecules and the calamitic LC groups in the side chains. This is an effect of so-called "soft epitaxy", which does not require lattice and molecular shape matching.

2.4. Linear Optical Properties of the Discotic Film via Modeling

In order to verify our structural analyses and their associations with the film optical properties, we also carried out optical modeling to calculate the linear optical properties of the DLC films. When light propagates through the DLC film having ordinary and extraordinary refractive indices n_0 and n_e, the *S* component (with polarization perpendicular to the incident plane) and the P component (with polarization in the incident plane) encounter different refractive indices and thus, have different optical lengths. The S component encounters the ordinary refractive index $n_{0,}$ and the angle between its propagation direction and the *z*-axis (the film surface normal) is given by

$$\alpha_1 = \sin^{-1}(\sin\alpha_0/n_0) \tag{1}$$

where α_0 is the angle of incidence outside the film. The *P* component encounters the effective refractive index n_{eff} as shown in Figure 9, which depends on the angle between the optical field *E* and the DLC director $\vec{n}$, and is given by

$$n_{eff} = \frac{n_e n_0}{\sqrt{n_e^2 \sin^2\beta + n_0^2 \cos^2\beta}} = \frac{n_e n_0}{\sqrt{n_e^2 \cos^2(\phi - \alpha_2) + n_0^2 \sin^2(\phi - \alpha_2)}} \tag{2}$$

where ϕ is the polar angle of the liquid crystal director $\vec{n}$, α_2 is the angle between the propagation direction, and the *z*-axis and can be found from

$$\alpha_2 = \sin^{-1}(\sin\alpha_0/n_{eff}) \tag{3}$$

The DLC columns in the ND phase are uniaxial around $\vec{n}$ and have a negative birefringence [$\Delta n = (n_e - n_0) < 0$]. Because $\vec{n}$ is a function of *z*, in our calculation, the film was divided into N slabs with thickness $\Delta z = h/N$. α_1 is a constant while α_2 is a function of *z*. The effective retardation of the film is given by

$$\Delta L_{eff} = \sum_{j=1}^{N} n_o(\Delta z/\cos\alpha_1) - \sum_{j=1}^{N} n_{eff}(\Delta z/\cos\alpha_2) + \left[\sum_{j=1}^{N}(\Delta z \tan\alpha_2) - \sum_{j=1}^{N}(\Delta z \tan\alpha_1)\right] \cdot \sin\alpha_0 \tag{4}$$

and ΔL_{eff} can be numerically calculated.

In the calculation, the following parameters were used: refractive indices of $n_e = 1541$, $n_o = 1.583$, the film thickness of $h = 1.6$ μm (as measured using atomic force microscopy (AFM)), and the assumed absolute value of surface angle of the DLC director $\vec{n}$ at the alignment layer surface was $\theta_s = 8.5°$ (as measured by SHG). The angle of the DLC director $\vec{n}$ at the

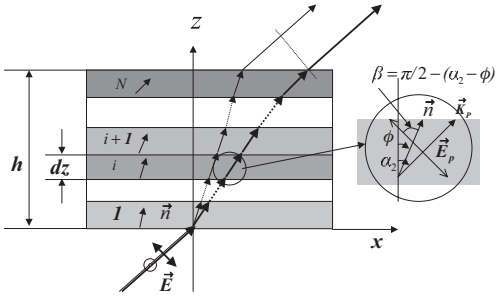

Fig. 9. A schematic drawing of the light propagation in an anisotropic optical film including S- and P-polarized light.

air interface θ_{air} was the only fitting parameter. As an approximation, the polar angle θ of $\vec{n}$ was assumed to vary linearly with respect to z. The calculated effective retardation is shown by the solid line in Figure 6. The best fit to the experimental data was obtained with the absolute value of $\theta_{air} = 27°$, which corresponds to the absolute value of an average angle $\theta_{om} = 17.8°$. The satisfactory fit of the optical modeling manifests the reliability of our deduction based on various experimental observations and confirms our microscopic understanding of the self-assembly mechanism of the DLCs on the alignment surface.

3. Conclusions

In summary, alignment layers with a high negative θ_b have been achieved in a newly designed polyimide containing cyanobiphenyl side chains (6FDA-11CBBP). The SHG and SERS experimental results provided evidence showing that on the molecular scale, a stable fold-like bent structure was formed by the cyanobiphenyl side chains of the polyimide. This structure was uniaxially anisotropic, and the CN groups preferentially pointed down towards the surface. As a result, the cyanobiphenyls in the fold-like bent structure generated the negative θ_s at the rubbed surface. Therefore, the high $-\theta_b$ of the bulk 5CB LCs (ca. –45°) was induced by the $-\theta_s$. When the UV-polymerizable DLC molecules were deposited on the alignment layer surface, this θ_s also induced a tilted orientation of the DLC molecules in the columnar nematic phase to form a negative retardation film with an oblique optical axis with $\theta_{om} = -18.6°$ and the $\theta_{air} = -29.1°$. This can be compared with calculated values of $\theta_{om} = -17.8°$ and $\theta_{air} = -27°$ based on optical modeling, which provides the best fit of the experimental results. The underlying molecular mechanism in forming this kind of negative retardation films was due to the fact that the DLC molecules were wedged onto the cyanobiphenyl side chains of the fold-like bent structure at the rubbed surface via an interaction with the cyanobiphenyl groups. An increase of the tilt angle θ of the DLCs with distance away from the rubbed surface (towards the air surface along the film surface normal) was attributed to a splay deformation of the DLC molecules along the film normal direction caused by surface anchoring energy changes.

4. Experimental

Materials and Sample Preparation: The polyimide was synthesized via a one-step polycondensation reaction of 2,2′-bis(3,4-dicarboxyphenyl)hexafluoropropane dianhydride (6FDA) and 2,2′-bis{ω-[4-(4-cyanophenyl)phenyoxy]-11-alkoxycarbonyl]}-4,4′-biphenyl diamine (11CBBP, where 11 is the number of methylene units in the side chains) [39], and abbreviated as 6FDA-11CBBP. Its chemical structure is shown in Figure 1. The intrinsic viscosity of this polymer was 0.56 dL g^{-1}, measured in chloroform at 30 °C. The glass-transition temperature was 110 °C, as measured using a differential scanning calorimeter (Perkin–Elmer DSC-7).

A series of reactive acrylic DLCs was synthesized with the general structure 2,3,6,7,10,11-hexakis(4′-acryloy-*m*-alkyloxybenzoyoxy)triphenylene [HAHBT-*m*, where *m* was the number of methylene units, and here $m = 6$ (HAHBT-6)] [40]. This full name of this DLC molecule was 2,3,6,7,10,11-hexakis(4′-acryloyhexyloxybenzoyoxy)triphenylene. The UV polymerizable DLC molecular structure is shown in the inset of Figure 2. The transmission level of an optical film constructed by these DLCs in the photonic region was generally measured above 90 % between 400 nm and 800 nm in a Lambda 19 (Perkin–Elmer) with a minimum of 85 % at 400 nm, as shown in Figure 2. The Fresnel optical reflection loss was estimated to be 9.3 % on both air–film sides, based on the equation of $I/I_0 = [(n-1)/(n+1)]^2$, where $n = 1.55$, I is the intensity of the reflected light, and I_0 is the intensity of the incident light [41]. The transition temperatures of HAHBT-6 were detected at a heating rate of 10 °C min^{-1} using DSC. The crystal melting temperature was at 104 °C (8.2 J g^{-1}) and the transition from the discotic nematic (DN) to the isotropic melt was at 173 °C (0.19 J g^{-1}). Thermal polymerization occurred between 140 °C and 173 °C, having a reaction enthalpy of 2.3 J g^{-1}. However, UV polymerization of HAHBT-6 was performed near or above the T_m.

The polyimide was dissolved in cyclopentanone at a concentration of 2 wt.-%, and the solution was filtered with a PTFE filter (0.45 μm). It was then spin-cast at 2000 rpm for 45 s on clean indium tin oxide (ITO) glass substrates (Fig. 3a). The thin layers were subsequently annealed at 100 °C for 1 h and then, at elevated temperature (200 °C) for an additional 1 h. The thickness was controlled in the range of 60–70 nm as measured using an atomic force microscope (Digital Instruments Nanoscope IIIa) in tapping mode. A thicker film sample (bulk sample) of approximately 40 μm that served as a reference in conventional FT-Raman measurements was also made by casting concentrated solutions.

Rubbing was conducted along one uniaxial direction using an automated rotating drum wrapped with velvet at room temperature. As illustrated in Figure 3b, the polyimide alignment layer passed through the drum along the translational direction. After rubbing, the alignment layer was again annealed at 200 °C for 1 h. The LC (5CB) molecules were filled into an assembled anti-parallel cell with 10 μm spacers in vacuum. The bulk LC θ_b in the cell was measured using a crystal rotation or a magnetic null method [42].

The DLC layer was assembled on the rubbed alignment surface via solution casting at a concentration of 15 wt.-% solid content in methyl ethylketone (Fig. 3c). After the evaporation of solvent at room temperature for 20 min, the discotic LC coating was dried at 100 °C for 10 min. The discotic film was then exposed to UV irradiation at 360 nm using a 300 W mercury lamp for 1 min at 105 °C under the protection of N_2 in order to carry out the crosslinking polymerization to stabilize the optical film (Fig. 3d).

Characterization Equipment and Experiments: The SERS measurements were conducted in a back-scattering geometry on a Bruker IFS 100 FT-Raman spectrometer equipped with a light source from an air-cooled Nd:YAG laser (1.064 μm) and a liquid nitrogen-cooled Ge detector. The chemical reduction reaction of $AgNO_3$ was involved in the preparation of the SERS-activated substrates. Ammonia and dilute formaldehyde solutions were subsequently added to the $AgNO_3$ solution to form suspended silver particles in the solution. The silver colloidal particles were then deposited onto the rubbed and unrubbed surfaces of the polyimide thin films. Finally, the SERS substrates were rinsed with 99.9 % ethanol and dried at room temperature so that rough SERS substrates formed with a high surface sensitivity.

In the SHG experiments, a frequency-doubled Q-switched mode-locked Nd:YAG laser at 532 nm was used as the fundamental input beam, and the SH reflection was detected at 266 nm after proper filtering. The incident angle was 67° with respect to the substrate plane normal on a rotation stage. SHG data was collected from four different input/output polarization combinations. The SHG experiment set-up was described elsewhere [30–32]. For SHG phase measurements, a fused quartz plate (1/8 in.; 1 inch ≈ 2.54 cm) was introduced as a phase modulator and a 50 μm thick z-cut quartz crystal plate (Q1) was used as a reference SH generator in the reflected beam path. The rotation of the fused quartz plate changed the optical path length and modulated the relative phase between the fundamental field and the reflected second harmonic field from the sample. The phase modulator caused the interference of SH fields from the sample and the reference quartz crystal (Q1) to produce an interference pattern. By comparing the interference pattern with one obtained from another crystalline quartz reference (Q2), the phase of $\vec{\chi}^{(2)}$ of the sample was reduced with respect to that of the quartz reference (Q2).

It was noted that we dealt with two sets of refractive indices in two systems. The first one was the refractive indices of the aligned DLC molecules. Their refractive indices were measured by casting the DLC molecules onto a flat surface with the disc cores aligned parallel to the surface. A Metricon 2010 optical prism coupler at 633 nm was used, and the in-plane refractive index ($n_0 = 1.583$) was obtained from the transverse electric (TE) mode and the out-of-plane refractive index ($n_e = 1.541$) was measured from the transverse magnetic (TM) mode. The second system utilized the films formed by DLC molecules on top of the alignment layer. Since the films possessed an oblique optical axis, the effective retardation value θL_{eff} of the film was measured via a Jones matrix using an ellipsometer at 633 nm in a transmission mode as a function of the incident angle (α_0) to identify the tilt optical axis of the optical film. In this set-up, the incident beam angle (α_0) was between the light beam and the normal of the film surface (z-axis) along the rubbing direction (x-axis) in the xz-plane. Therefore, the effective retardation was measured by the ellipsometer coupled with a ±45° rotating stage at an interval of every 5° (at an accuracy of ±0.5°). Similarly, one could also measure the effective retardation as a function of the incident angle (α_0) perpendicular to the rubbing direction (y-axis) in the yz-plane.

Two-dimensional (2D) WAXD fiber experiments were conducted on a Rigaku 18 kW rotating anode generator ($\lambda = 0.1542$ nm, Cu Kα) coupled with an image plate. The reflection peak positions and widths observed were calibrated using silicon crystals of known crystal sizes in the high-angle region ($2\theta > 15°$) and silver behenate in the low-angle region ($2\theta < 15°$). 2 h exposure times for the thin film was required in order to obtain a high quality pattern.

Received: February 26, 2003
Final version: May 30, 2003

[1] P. J. Bos, D. Fredley, J. Li, J. Rahman, *Liquid Crystals in Complex Geometries* (Eds: G. P. Crawford, S. Zumer), Taylor and Francis, London **1996**, pp. 281–289.
[2] S. Morozumi, *Liquid Crystals* (Ed: B. Bahadur), Vol. 1, World Scientific Publishing, Singapore **1990**, pp. 171–194.
[3] D. J. Broer, J. Lub, G. N. Mol, *Nature* **1995**, *378*, 467.
[4] R. A. M. Hikmet, J. Lub, A. J. Tol, *Macromolecules* **1995**, *28*, 3313.
[5] T. Miyashita, Y. Yamaguchi, T. Uchida, *Jpn. J. Appl. Phys.* **1993**, *34*, L177.
[6] M. Schadt, H. Seiberle, A. Schuster, *Nature* **1996**, *380*, 212.
[7] R. A. Soref, *J. Appl. Phys.* **1974**, *45*, 5466.
[8] S. Chandrasekhar, B. K. Sadashiva, K. A. Suresh, *Pramana* **1977**, *9,* 471.
[9] D. Adam, F. Closs, T. Grey, D. Funhoff, D. Harrer, H. Ringsdorf, P. Schuhmacher, K. Siemensmeyer, *Phys. Rev. Lett.* **1993**, *70*, 457.
[10] D. Adam, P. Schuhmacher, J. Simmerer, L. Häusaaling, K. Siemensmeyer, K. H. Eztbach, H. Ringsdorf, D. Harrer, *Nature* **1994**, *371*, 141.
[11] J. Simmerer, B. Glusen, W. Paulus, A. Ketter, P. Schuhmacher, D. Adam, K. H. Etzbach, K. Siemensmeyer, J. H. Wendorff, H. Ringsdorf, D. Harrer, *Adv. Mater.* **1996**, *8*, 815.
[12] D. Wöhrle, D. Meissner, *Adv. Mater.* **1991**, *3*, 129.
[13] L. Schmit-Mende, A. Fechtenkotter, K. Müllen, E. Moons, R. Friend, J. D. Mackenzie, *Science* **2001**, *293*, 1119.
[14] T. Christ, B. Glusen, A. Greiner, A. Ketter, H. Sander, V. Stumpflen, V. Tsukruk, J. H. Wendorff, *Adv. Mater.* **1997**, *9*, 48.
[15] C. Destrade, H. T. Nguyen, H. Gasparoux, J. Malhtate, A. M. Levelut, *Mol. Cryst. Liq. Cryst.* **1981**, *71*, 111.
[16] C. Pugh, V. Percec, *J. Mater. Chem.* **1991**, *1*, 765.
[17] F. Ciuchi, G. D. Nicola, H. Franz, G. Gottarelli, P. Mariani, M. G. Bossi, G. P. Spada, *J. Am. Chem. Soc.* **1994**, *116*, 7064.
[18] N. Boden, R. J. Bushby, N. Cammidge, *J. Am. Chem. Soc.* **1995**, *117*, 924.
[19] N. Boden, R. J. Bushby, G. Cooke, O. R. Lozman, Z. Lu, *J. Am. Chem. Soc.* **2001**, *123*, 7915.
[20] J. Y. Chang, J. H. Baik, C. B. Lee, M. J. Han, *J. Am. Chem. Soc.* **1997**, *119*, 3197.
[21] B. Y. Tang, J. J. Ge, A. Zhang, B. Calhoun, P. Chu, H. Wang, Z. Shen, F. W. Harris, S. Z. D. Cheng, *Chem. Mater.* **2001**, *13*, 78.
[22] M. Kardan, B. B. Reinhold, S. L. Hsu, R. Thakur, C. P. Lillya, *Macromolecules* **1986**, *19*, 616.
[23] M. Kardan, K. Akira, S. L. Hsu, R. Thakur, C. P. Lillya, *J. Phys. Chem.* **1987**, *91*, 1809.
[24] C. D. Favre-Nicollin, J. Lub, P. V. A. Sluis, *Adv. Mater.* **1996**, *8*, 12.
[25] C. D. Favre-Nicollin, J. Lub, *Macromolecules* **1996**, *29*, 6143.
[26] H. Mori, Y. Itoh, Y. Nishiura, T. Nakamura, Y. Shinagawa, *Jpn. J. Appl. Phys.* **1997**, *36*, 143.
[27] K. Kawata, M. Okazaki, *US Patent 2 218 783*, **1996**.
[28] M. Okazaki, K. Kawata, H. Nishikawa, M. Negoro, *Polym. Adv. Technol.* **2000**, *11*, 398.
[29] K. Kawata, *Chem. Rec.* **2002**, *2*, 59.
[30] M. B. Feller, W. Chen, Y. R. Shen, *Phys. Rev.* A **1993**, *43*, 6778.
[31] X. Zhuang, L. Marrucci, Y. R. Shen, *Phys. Rev. Lett.* **1994**, *73*, 1513.
[32] X. Wei, X. Zhuang, S.-C. Hong, T. Goto, Y. R. Shen, *Phys. Rev. Lett.* **1999**, *82*, 4256.
[33] J. J. Ge, C. Y. Li, G. Xue, I. K. Mann, D. Zhang, S.-Y. Wang, F. W. Harris, S. Z. D. Cheng, S.-C. Hong, X. Zhuang, Y. R. Shen, *J. Am. Chem. Soc.* **2001**, *123*, 5768.
[34] S.-C. Hong, M. Oh, X. Zhuang, Y. R. Shen, J. J. Ge, F. W. Harris, S. Z. D. Cheng, *Phys. Rev. E* **2001**, *63*, 0 517 061.
[35] J. J. Ge, G. Xue, F. Li, K. W. McCreight. S-Y. Wang, F. W. Harris, S. Z. D. Cheng, S.-C. Hong, X. Zhuang, Y. R. Shen, *Macromol. Rapid. Commun.* **1998**, *19*, 619.
[36] P. Hendra, C. Jones, G. Warnes, *Fourier Transform Raman Spectroscopy*, Ellis Horwood, Hemel Hempsted, UK **1991**.
[37] M. Moskovits, *J. Chem. Phys.* **1982**, *77*, 4408.
[38] K. Ichimura, S. Furumi, S. Morino, M. Kidowaki, M. Nakagawa, M. Ogawa, Y. Nishiura *Adv. Mater.* **2000**, *12*, 950.
[39] S.-Y. Wang, *Ph.D. Thesis*, The University of Akron, OH **1995**.
[40] F. Bai, *Ph.D. Thesis*, The University of Akron, OH **2000**.
[41] J. H. Simmons, K. S. Potter, *Optical Materials*, Academic Press, San Diego, CA **2000**.
[42] T. J. Scheffer, J. Nehring, *J. Appl. Phys.* **1977**, *48*, 1783.

